PRIFYSGOL

BANGOR

UNIVERSITY

Realistic wave conditions and their influence on quantifying the tidal stream energy resource

Lewis, M.J.; Neill, S.P.; Hashemi, M.R.

Applied Energy

Cyswllt i'r cyhoeddiad / Link to publication

13. Mar. 2024

Realistic wave conditions and their influence on quantifying the tidal stream energy resource

CrossMark

M.J. Lewis *, S.P. Neill, M.R. Hashemi, M. Reza

Bangor University, School of Ocean Sciences, Menai Bridge LL59 5AB, United Kingdom

HIGHLIGHTS

- Waves are frequently aligned at an oblique angle to the tidal current.
- Wave angle must be considered for realistic oceanographic conditions.
- Waves have a significant impact on the tidal stream energy resource.
- The net tidal resource is reduced by ∼10% per metre wave height increase.

ARTICLE INFO

ABSTRACT

When selecting suitable sites for tidal stream energy arrays a wide range of factors must be considered, from the magnitude of the tidal stream resource, to realistic oceanographic conditions. Previous computational and laboratory-scale investigations into the impact of waves upon tidal turbines (such as turbine blade loadings) and turbine arrays (such as array configuration) typically assume that waves propagate "*inline*" to the tidal current (waves following or waves opposing the tidal current with a 20° tolerance limit). We investigated the wave climate at typical tidal stream energy sites across the British Isles. The wave climate was simulated at 18 sites using a 7-year (2005–2011) SWAN wave model simulation of the northwest European shelf seas. The principal semi-diurnal lunar constituent (M2) was also estimated at these sites using the three-dimensional ROMS tidal model. A significant proportion of the wave climate (between 49% and 93% of the time), including extreme wave events (>10 m wave heights), was found to be propagating in a direction which was "oblique" to the major axis of tidal flow (i.e. waves which propagate at an angle to the tidal current with a 20° tolerance limit) at all 18 selected sites. Furthermore, the average "*inline*" wave climate was 2.25 m less in height and 2 s less in wave period in comparison to the oblique wave climate. To understand the direct effect of waves upon the tidal stream resource, the dynamically wave-tide coupled COAWST modelling system was applied to an idealized headland case study, which represented the typical tide and wave conditions expected at first generation tidal stream energy sites. Waves were found to alter the simulated tidal velocity profile, which, because tidal stream power is proportional to velocity cubed, reduced the theoretical resource by 10% for every metre increase in wave height (R^2 94% with *22 degrees of freedom*) – depending upon wave period and direction. Our research indicates that wave angle should be considered when quantifying the impact of waves upon tidal turbines, such as computational fluid dynamic (CFD) studies, or laboratory-scale experiments of wake characteristics and turbine fatigue loading. Further, dynamically coupled tide-wave models may be necessary for a thorough resource assessment, since the complex wave-tide interaction affected the tidal resource; however, in situ observations of tidal velocity profiles during a range of wave events will be essential in validating such modelling approaches in the future.

1. Introduction

Accurate assessment of the power available for electricity generation at tidal stream energy sites is essential for successful device deployment. For example, the local wave climate may render some tidal energy sites inefficient. A number of marine renewable

---

* Corresponding author.
 E-mail address: m.j.lewis@bangor.ac.uk (M.J. Lewis).

energy sites are now being developed around the world, and so understanding realistic oceanographic conditions at proposed tidal stream energy sites is a priority for the industry; such that operability, survivability and reliability can be optimised.

The tidal stream resource in the UK is substantial, with an estimated 30% of all UK electricity demand that could theoretically be produced by tidal power alone [1]. Further, there is a considerable wave energy resource in UK waters (e.g., [2]), however this energetic wave climate may affect the tidal energy resource [3–5]. The impact of tides on the practical wave energy resource has recently become the focus of research (e.g. [6,7]), whilst, we find, the majority of academic studies on tidal stream energy does not adequately account for realistic waves; therefore, the impact of waves on the tidal stream energy resource is the focus of this current work.

Variability within the tidal current (for example, turbulence and the velocity profile) results in variability to the loadings upon the support structure, the tidal turbine and the gearbox – hence increasing potential failure and reducing potential performance [8–10]. Over-engineering is likely to affect the viability of commercial tidal stream energy projects (e.g., [11]) whilst, conversely, maintenance is likely to be costly and difficult (e.g. [12]). Indeed, O'Rourke et al. [13] highlighted that current restrictions to tidal stream energy development were installation, maintenance, and loading conditions. The addition of wave forces and momentum will increase fatigue and loadings that could increase the potential damage to the tidal turbine and its support structure (e.g., [14–16]); therefore, the implications of wave loading upon tidal stream devices, in terms of fatigue and turbine spacing (within an array), has rightly become the focus of recent research [17,18]. Additionally, the amount of time when the tidal turbine cannot produce power (which we call downtime) could have a significant effect upon the viability of a site. Further, the period of extreme storm waves and sea-states that may interrupt maintenance programs should be considered when selecting potential tidal stream energy sites.

A major assumption within research of surface wave loading upon tidal stream turbines is that wave propagation is aligned with the rectilinear tidal flow; with either "waves following" (propagating with the tidal current), or "waves opposing" (propagating against the tidal current). As waves propagate into coastal waters, shallow water processes transform their height (H), period (T) and direction (θ) [19], such as shoaling and refraction due to bathymetric features. During extreme storm events, waves above 18 m in height have been observed in UK waters [20], which may have been the result of a crossing sea state of two crossing (by at least 90°) wave groups [21]; hence, it appears that waves can propagate at angle to the tidal current direction, and in doing so can become highly nonlinear, which may be an important consideration within tidal stream energy design.

Tidal current misalignment to the turbine has been shown to increase the loading and failure potential of a turbine (e.g. [22]); hence wave – tidal current misalignment is likely to further increase the fatigue and extreme loadings of a tidal turbine. Furthermore, as turbulence and wave processes affect the thrust, torque, and tip-loss/stall characteristics of turbine blades [8,23], the effect of *oblique* wave events is likely to affect turbine performance, wake properties (hence array configuration), and fatigue loading estimates. Events when waves cross sea currents are well documented [24,25] – yet the occurrence of oblique wave events at potential tidal stream energy sites has yet to be quantified. Indeed, within the tidal stream energy literature, we could find no studies of wave impacts upon tidal turbines which included wave angle; either *via* laboratory studies (e.g. [18]) or computational fluid dynamic (CFD) modelling (e.g., [15,26]). We hypothesise that there will be many instances when waves will not propagate *inline* to the

tidal flow (waves following or waves opposing the tidal flow); hence a significant *oblique* wave climate may be present at a proposed tidal stream energy site (i.e. times when waves are travelling at an angle that is oblique to the rectilinear tidal flow).

Surface waves add additional momentum and mass to the mean flow in the form of Stokes velocities, and the generation of radiation stresses [27]. Further, surface waves significantly affect the apparent bed roughness felt by the tidal flow near the bed, due to turbulent momentum transfer of these higher frequency oscillatory wave velocities [28–30]. Hence, surface waves can have a considerable influence on mean velocity profiles in coastal waters (e.g., [31]). Excluding inter-device interactions, device characteristics (e.g. cut-in and power-rated velocities), and tidal flow by-pass [32], the tidal stream power density is approximately proportional to the cube of the tidal velocity (e.g. [33]); thus any small change in tidal flow could result in a significant change in the available tidal resource. Furthermore, when we consider instances when electricity is not generated due to storm waves, or periods of calm sea-state suitable for maintenance work, the local wave climate could have a significant impact on the annual net power available at a proposed tidal stream energy site.

Non-linear interactions between waves and currents, in a coastal setting, have been the focus of much research over the last decade [30], including the effects of tides on modifying the wave energy resource [6]. However, little research has been performed on the effect of waves on the tidal stream resource. Observations from flume experiments (e.g., [34,35]) and CFD models (e.g., [29]), show an increase in upper water-column velocities occurs when waves propagate in the opposite direction to the tidal flow – whilst the converse is true when waves propagate in the same direction as the tidal currents. The specific effect of surface waves on the velocity profile is dependent on bed roughness and wave angle; for example, an increase in near bed tidal velocities was found when waves are propagating in a direction that is perpendicular to the tidal current for a smooth bed, with the opposite occurring (reduction in near bed velocity) when the bed is rough [34–37]. Nevertheless, the apparent bed roughness (the seabed friction experienced by the tidal flow due to the physical bed roughness combined with the relative roughness which is a function of the wave orbital velocity) is the dominant factor in wave-current interaction processes (e.g. [28–30,37,38]). However, the net effect over a tidal cycle is that the presence of waves can increase the apparent bed roughness (experienced by the tide), which reduces depth averaged tidal velocities (albeit slightly), and alters the velocity profile (e.g. [37–39]).

In shallow-water coastal regions, and at times of major storm wave events, the effect of wave-current interaction can be significant [38]. Observations by Prandle and Wolf [39] in 12.5 m water depth found that the depth averaged speed of the principal semi-diurnal lunar constituent (M2) decreased by 5% with each 1 m increase in wave height (wave direction unknown) – which we call the Prandle and Wolf relationship in this paper. Although modification of bottom friction reportedly had little effect on depth averaged tidal currents in water depths greater than 50 m [40], most turbines will likely be deployed in water depths less than 50 m [41]; hence, the direct effect of surface waves on the tidal resource may be significant.

As an example, we can estimate the change in the tidal stream power available if the presence of waves reduces the depth averaged peak tidal velocity ($\bar{u}$) by 0.1 m/s – from 2 m/s to 1.9 m/s (which equates to a 2 m wave height based on the Prandle and Wolf relationship [39]). The net power density (P) can be estimated over a tidal cycle assuming $\int_0^{12.42\,\text{h}} P_t = \frac{1}{2}\rho(\bar{u}_t)^3 dt$ (where $\rho = 1025$ kg/m³) and the sinusoidal tidal velocity ($\bar{u}_t$) has a period of 12.42 h. In our example, we estimate the total net power density

available over a tidal cycle reduces from 21.6 kW/m^2 to 18.5 kW/m^2 if the depth averaged tidal velocity decreases by 0.1 m/s; a 14% reduction in the resource.

The aim of this paper is to examine the wave climate at a number of proposed tidal stream energy sites around the British Isles, including wave direction, and to discuss the likely impacts on the tidal energy resource; thus determining if a computationally expensive coupled wave-tide modelling approach is necessary to fully characterize the tidal energy resource. Firstly we establish the *oblique* wave climate at selected tidal stream energy sites (Section 2). We then use a dynamically coupled wave-tide model to understand the impact of waves upon the power available at a typical 1st generation tidal stream energy site (Section 3).

We have chosen to use a 3-dimensional hydrodynamic model system with hydrostatic approximations (see Section 2.1) because we need to accurately determine the major axis of tidal current propagation at tidal stream energy sites where secondary flows may be important (for comparison to wave climate direction – see Section 2), and simulate at spatial scales (and regions) where vertical accelerations are negligible in comparison to gravitational accelerations. Moreover, we use a 3-dimensional dynamically coupled (wave-tides) modelling system because we are interested in the effect of waves on the velocity profile of tidal flow (Section 3); however, it should be noted that other modelling approaches exist (e.g. [41,42]), each with benefits and penalties.

2. Wave and tide directionality

To understand the wave climate at a typical potential tidal stream site, we employed a 7-year spectral wave model, and a 28-day 3D tidal model to resolve the main spring-neap tidal ellipse constituents (the combination of the principal semi-diurnal solar constituent, S2, and the M2 constituent, defined already, describes the UK's spring-neap cycle). The tide and wave models were run independently in this section, and the directional wave climate was compared to the angle of the major axis of the tidal ellipse. Therefore, the directional wave climate relative to the tidal flow at a number of potential tidal stream energy sites around the British Isles was calculated.

2.1. Tidal model

To simulate the tidal flow around the British Isles, the 3D Regional Ocean Modelling System (ROMS) model [43–45] was used – a modelling system that has been successfully applied to tidal stream energy studies in the UK (e.g., [46]). ROMS is a free-surface ocean circulation model, based on finite-difference approximations of the Reynolds-Averaged Navier–Stokes (RANS) equations using hydrostatic and Boussinesq assumptions, with terrain-following (sigma) coordinates in the vertical, and orthogonal curvilinear coordinates in the horizontal [47]. Further details about the model code can be found here: https://www.myroms.org.

The GEBCO bathymetric data product (http://www.gebco.net/), at 30 arc-second resolution, was used to construct a regular 1/24° horizontal resolution model domain extending from 42°N to 62°N, and from 15°W to 10°E (see Fig. 1), with ten depth layers using the sigma coordinate system (evenly distributed throughout the water column). The open boundary was forced with TPXO7 data (http://volkov.oce.orst.edu/tides/TPXO7.2.html) for ten tidal constituents (M2, S2, N2, K2, K1, O1, P1, Q1, Mf, and Mm). A computational time step of 60 s (barotropic) was used for a 30 day simulation (including 2 days of spin-up) with a minimum water depth of 10 m. Wetting and drying was not included in this simulation, as the geographic scale of inter-tidal regions was negligible in relation to the model resolution at shelf scale. The Generic Length Scale
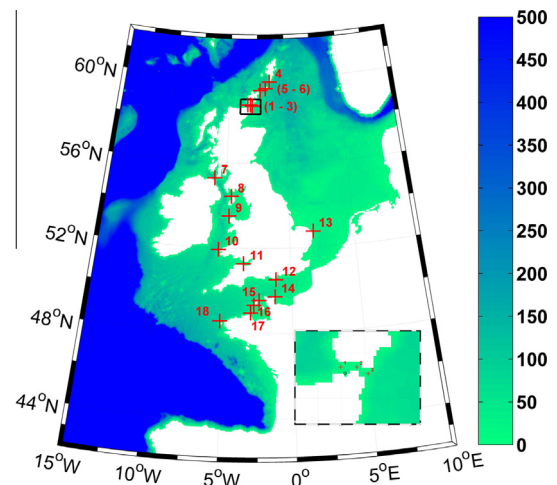
Fig. 1. The computational domain and bathymetry (colour scale in metres) of the 3D ROMS tidal model, with 18 potential tidal stream energy sites (shown as red crosses) where the amplitude of the principal semi-diurnal lunar (M2) velocities exceed 1.5 m/s. An expanded view (black box) of the Pentland Firth (sites 1 to 3), with the location of the wave buoy shown as a black circle. (For interpretation of the references to colour in this figure legend, the reader is referred to the web version of this article.)

(GLS) model for simulating turbulence was set to the κ-ε turbulence model for our simulations ($p = 3$, $m = 1.5$ and $n = -1$ – for further details see [48]). Furthermore, it should be noted that similar results were found when a number of ROMS turbulence schemes and a number of case studies were investigated [48]. Quadratic friction was employed with a drag coefficient (Cd) of 0.003, which is consistent with previous ROMS studies that simulate the flow through energetic tidal channels (e.g., [46]).

Validation of our ROMS tidal model was performed for M2 and S2 elevation components (amplitude and phase), at 45 tide gauges around the British Isles – from the National Tidal and Sea Level Facility (www.ntslf.org). A Root-Mean-Squared-Error (RMSE) of 0.30 m (normalized RMSE of 7%), and a phase RMSE of 13° was calculated for the validation of the M2 constituent. A RMSE of 0.08 m (6% normalized RMSE) and 21° was calculated for the validation of the amplitude and phase of the S2 constituent. The skill of our tidal model was validated using a linear regression score (R^2) and a Pearson's correlation score of the dependence, between observed and simulated M2 and S2 elevations at the 45 tide gauges. An R^2 value of 94% and Pearson's correlation coefficient of 0.97 for the M2 constituent was calculated (at 5% level of significance). For the S2 constituent, an R^2 value of 96%, and Pearson correlation coefficient of 0.98 was calculated. Therefore, we found our 1/24° ROMS tidal model showed accuracy and skill at simulating the sea-level associated with the spring-neap cycle.

M2 tidal ellipse information from our model was compared to the Finite Element Solution and data assimilated global tide product; FES2012 [49,50]. As a data assimilated product, FES2012 validates extremely well [49,50]; however, many important tidal energy sites (e.g. the Pentland Firth; sites 1 to 3) are not resolved within this tidal data product due to the spatial resolution (which is 1/16°). To gain confidence in the tidal velocities simulated in our ROMS tidal model, we compared FES2012 M2 ellipse information at 11 of the sites in Table 1 (as the 7 other sites were not resolved sufficiently by the FES2012 product). Comparison to the FES2012 M2 tidal ellipse information gave a RMSE of 7° for the M2 ellipse inclination (angle of the major tidal current axis), and an M2 phase RMSE of 9°. Therefore, we assume the direction of our tidal velocities in the ROMS tidal model to be accurate.

Table 1

The location and estimated depth-averaged M2 tidal ellipse information for 18 potential tidal stream energy sites distributed around the British Isles, calculated using a ROMs tidal model. Tidal ellipse inclination is displayed as the angle (clockwise from North) to the major axis component, with the maximum (Cmax) and minimum (Cmin) velocity axis also shown.

Site	Site description	Latitude (°N)	Longitude (°East)	Cmax (m/s)	Cmin (m/s)	Inclination (°N)
1	Pentland Firth – west	58.73	−3.34	2.25	0.05	274
2	Pentland Firth – central	58.73	−3.11	3.59	−0.18	286
3	Pentland Firth – east	58.68	−2.95	2.32	−0.36	303
4	Shetland south	59.80	−1.40	1.34	−0.15	301
5	Fair Isle	59.49	−1.76	1.52	−0.29	328
6	Orkney – north	59.41	−2.24	1.85	−0.10	323
7	Islay	55.28	−5.99	3.00	−0.14	319
8	Isle of Man	54.44	−4.58	1.94	−0.08	60
9	Anglesey	53.51	−4.73	1.84	−0.17	52
10	Pembroke	51.93	−5.45	1.61	−0.02	32
11	Bristol channel	51.29	−3.53	1.52	−0.03	287
12	Isle of Wight	50.53	−1.12	1.56	−0.04	87
13	East Anglia	52.75	1.84	1.55	−0.05	326
14	Cherbourg east	49.73	−1.20	1.82	0.04	306
15	Alderney north	49.56	−2.37	2.14	0.28	323
16	Alderney south	49.34	−2.75	1.74	0.30	314
17	Northern Brittany	48.97	−2.98	2.39	−0.03	308
18	Southern Brittany	48.57	−5.16	1.83	−0.28	56

2.2. Wave model

Surface waves were modelled independently of the tide using the SWAN (Simulating WAves Nearshore) third-generation spectral wave model [51]. We used a SWAN wave model of the northwest European shelf sea that has already been extensively validated [2,52]. The wave model was applied initially to a region which covered the entire North Atlantic at a grid resolution of 1/6°, extending from 60°W to 15° E and from 40°N to 70°N. A one-way nested higher resolution (1/24°) grid of the same domain as the UK ROMS tidal model (see Fig. 1) allowed the wave climate of potential tidal stream energy sites to be resolved sufficiently. The wave climate of the northwest European shelf sea was simulated for a 7 year period (2005–2011), using Met Éireann (the Irish Meteorological Service) gridded wind data from their operational HIRLAM (High Resolution Limited Area Model) version 7.2 forecast model (www.hirlam.org). The grid resolution of this HIRLAM model is 0.1°, with 60 vertical levels, and the resolution of the interpolated output wind data is 0.5°, extending from 60°W to 15°E, and from 40°N to 70°N at 3-hourly intervals.

2.3. Current and wave angle comparison methodology

The major (Cmax) and minor (Cmin) axes of peak M2 tidal velocity in a tidal ellipse describes the size and shape, with phase describing the timing of peak currents. Hence, the angle of the rectilinear (or near-rectilinear) M2 tidal flow at potential tidal stream energy sites is the angle (INC) of the major tidal current axis (Cmax). The descriptive parameters (Cmax, Cmin, INC and phase) of the major semi-diurnal lunar constituent (M2) depth-averaged tidal ellipse were calculated using t_tide analysis [53] from the 28 day ROMS simulated depth-averaged tidal velocities (2 days allowed for model spin up). A 28-day simulation was chosen to accurately infer the M2 (principal semi-diurnal lunar constituent) and S2 (principal semi-diurnal solar constituent) tidal constituents. A number (but not an exhaustive list) of proposed tidal stream energy sites around the British Isles was identified (Table 1 and Fig. 1) based on regions where the amplitude of our ROMS simulated depth-averaged M2 Cmax was greater than 1.5 m/s, and the peak spring-neap (M2 + S2) tidal current exceeded 2 m/s – a threshold that is desirable for tidal stream energy extraction.

The 7-year (2005–2011) time-series of the 3-hourly simulated wave climate was extracted at these 18 potential tidal stream energy sites (see Fig. 1 and Table 1). The angle of wave direction (travelling from, °N) was compared to the simulated inclination of the M2 major current axis (also calculated relative to °N). If wave propagation was within ±20° to INC (flood tide flow), or the reverse of this angle (ebb flow), then the wave event was considered to be "inline" – waves propagating with or against the tidal current. A directional uncertainty of ±20° was included to account for resolution errors within the models (we estimated 20° to be the maximum sub grid-scale refraction possible at the 18 selected sites in our simulations), as well as processes not resolved within the tide or wave model; such as wave refraction due to tidal currents (e.g. [24,25]). Generally, shorter period waves are mainly affected by tidal current refraction [7], whilst longer period swell waves (with wave orbital motion that penetrate further into the water-column) are more affected by bathymetry refraction. Therefore *inline* (±20°) wave events could be identified within the 7-year SWAN simulation, and the *oblique* wave climate can also be calculated (assuming a device always faces the direction of tidal flow).

2.4. Current and wave angle comparison results

The 7-year (2005–2011) wave climate at the 18 selected sites (Fig. 1) is shown in Table 2, simulated with the well validated [2,52] SWAN model of the northwestern European shelf seas. The simulated wave period we present (displayed in Table 2) is the mean absolute wave period (*TM02*); defined as $TM02 = 2\pi \left(\frac{\iint \omega^2 E(\omega,\theta)\delta\omega\delta\theta}{\iint E(\omega,\theta)\delta\omega\delta\theta} \right)$ within the SWAN derived energy density spectrum $E(\omega,\theta)$ of the relative radian frequency (ω) distributed over direction (θ) – which gives the most comparable measure of wave period with wave buoy observations [54]. To describe the simulated wave height, the well-known significant wave height parameter (*Hs*) was used, based on the variance of the sea surface elevation (m_0) as $Hs = 4\sqrt{m_0}$.

The wave climate across the 18 selected sites was found to have similar mean wave heights (of order 1–2 m, and wave periods between 3 and 4 s; see Table 2. However, there is spatial variability, and west coast bias, in the magnitude of the wave climate around the British Isles (Table 2). For example, the simulated maximum reduces by approximately 3 m between the west (site 1) and the east (site 3) of the Pentland Firth (see Fig. 1), with a small

Table 2
The maximum and mean wave climate, including standard deviation (s.d.), of wave height (Hs) and period (T) simulated between 2005 and 2011 at 18 potential tidal stream energy sites. Frequency of "maintenance widows" was calculated as the number (%) of calm days when wave height was less than 2 m.

Site	Mean wave climate		s.d. of wave climate		Maximum		Maintenance window (% of record <2 Hs)
	Hs (m)	T (s)	Hs (m)	T (s)	Hs (m)	T (s)	
1	1.38	2.7	1.04	1.0	9.59	8.7	79
2	1.13	2.4	0.78	0.8	7.08	7.4	87
3	1.15	2.5	0.75	0.7	6.53	6.4	88
4	2.06	3.2	1.41	1.0	11.91	8.1	59
5	2.05	3.2	1.41	1.0	11.70	8.0	60
6	1.97	3.1	1.30	0.9	9.79	7.5	61
7	1.20	2.4	0.88	0.8	7.34	6.2	85
8	0.92	2.1	0.68	0.7	4.89	4.9	92
9	1.22	2.4	0.96	0.9	7.66	6.2	82
10	1.50	2.7	1.17	1.0	10.40	7.5	75
11	0.81	2.0	0.65	0.8	5.78	6.3	94
12	1.16	2.3	0.95	0.9	9.15	7.6	85
13	0.98	2.2	0.64	0.7	5.12	5.4	93
14	0.83	2.0	0.57	0.6	4.35	4.5	95
15	1.10	2.3	0.78	0.7	8.02	6.6	88
16	1.32	2.5	1.01	0.9	11.09	7.9	81
17	1.25	2.5	0.88	0.8	9.70	7.5	84
18	1.73	3.0	1.28	1.1	12.49	8.4	69

change in the mean wave height (and associated standard deviation).

The majority (i.e. nine sites: 1, 4, 5, 6, 10, 12, 16, 17 and 18) of the 18 selected sites experienced extreme wave events in the 7-year simulation that exceeded 9 m in height and 7.5 s in period. Moreover, the significant wave height (Hs) and mean absolute wave period (which we shall call T from here) are statistical properties, therefore sites will experience individual waves greater than the values in Table 2. Relatively quiescent wave conditions, when compared to other selected locations such as sites 4 and 5 (see Table 2), were found at sites 8 (Isle of Man), 13 (East Anglia) and 14 (Cherbourg east); which all had a maximum wave event less than 5.5 m at 5.5 s, and a mean Hs below 1 m.

The amount of time access for maintenance can be achieved may be an important consideration when selecting a tidal stream energy location. A maintenance window was calculated as the percentage of time (within the 7 year simulation), when Hs was <2 m. A wave height of 2 m was chosen as the threshold of a "calm" day based on offshore wind farm guidance for maintenance boat access

Fig. 2. Significant wave height (Hs in metres) exceedance probability (%) of four contrasting potential tidal stream energy sites (sites 1, 4, 10, and 14 see Table 1) – estimated using a 7-year SWAN wave model of the northwest European shelf sea. The 2 m wave height "maintenance window" threshold is shown as a black dashed line.

[55] – however, the significant wave height exceedance probabilities for a number of sites (1, 4, 10, and 14) is shown in Fig. 2 to demonstrate the variability of "maintenance windows" (irrespective of a wave height threshold) between sites. Sites 1 and 10 (see Fig. 2) were found to have a significant wave height climate close to the average (see Table 2), whilst site 4 had the largest wave climate and 14 had a quiescent wave climate (see Fig. 2). Further, sites 4, 5 and 6 (i.e. the Northern Isles of Scotland) were found to have a low number of "maintenance window" periods during the 7-year simulation (~60%), especially when compared to some other tidal sites where waves were below 2 m for over 90% of the time (e.g. sites 8, 11, 13 and 14: see Table 2).

The inclination (i.e. angle) of the major axis of the depth averaged M2 tidal current ellipse was compared to the simulated 7-year wave climate (2005–2011) at each of the 18 selected sites. As an example, the directional wave climate (wave height an period), compared to the tidal current output and M2 tidal ellipse for three selected sites is shown in Fig. 3, which demonstrates that wave events were not always *inline* to the M2 major tidal current axis. The *inline* wave climate was calculated when simulated wave directions were following or opposing the ROMS simulated M2 tidal peak current direction (M2 inclination ±20°). Hence, as described in Fig. 3 for a three sites, the wave climate *inline* to the major tidal current axis can be determined. The *inline* wave climate (waves following or waves opposing the M2 tidal current ±20°) for all 18 selected sites is shown in Table 3, whilst the oblique wave climate (waves that are not propagating *inline* with the rectilinear tidal flow) is shown in Table 4. As an example, in the first entry of Table 3 (site 1); waves were *inline* with the tidal flow for 33% of the 7-year period, with a mean *inline* Hs of 1.58 m and T of 3.8 s. In contrast, waves were oblique to the tidal current 67% of the 7-year period at site 1 (see Table 4), with a mean oblique Hs of 1.29 m and T of 3.3 s.

The *inline* wave climate varied significantly between the selected tidal stream energy sites (Table 3). Moreover, the wave climate *oblique* to the tidal flow was found to be greater than the *inline* wave climate at all 18 selected sites with the exception of site 11 (the Bristol Channel); see Table 4. This is not surprising, since tidal currents tend to be aligned parallel to the coastline, whereas waves will refract towards the coastline according to their wave period, such that a typical wave orthogonal will be perpendicular to the coastline. For example, sites in Islay (site 7) and Pembroke (site 10) had an *oblique* wave climate over 90% of the time between 2005 and 2011 (see Table 4). Indeed, the *oblique* wave climate on average (between all 18 sites) accounted for 59% of the 7-
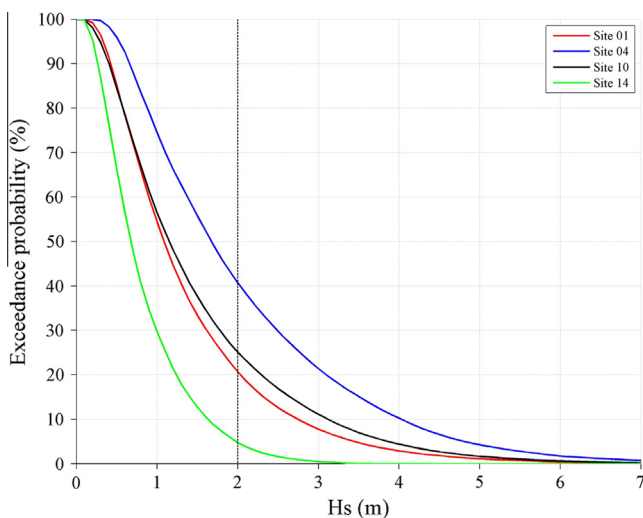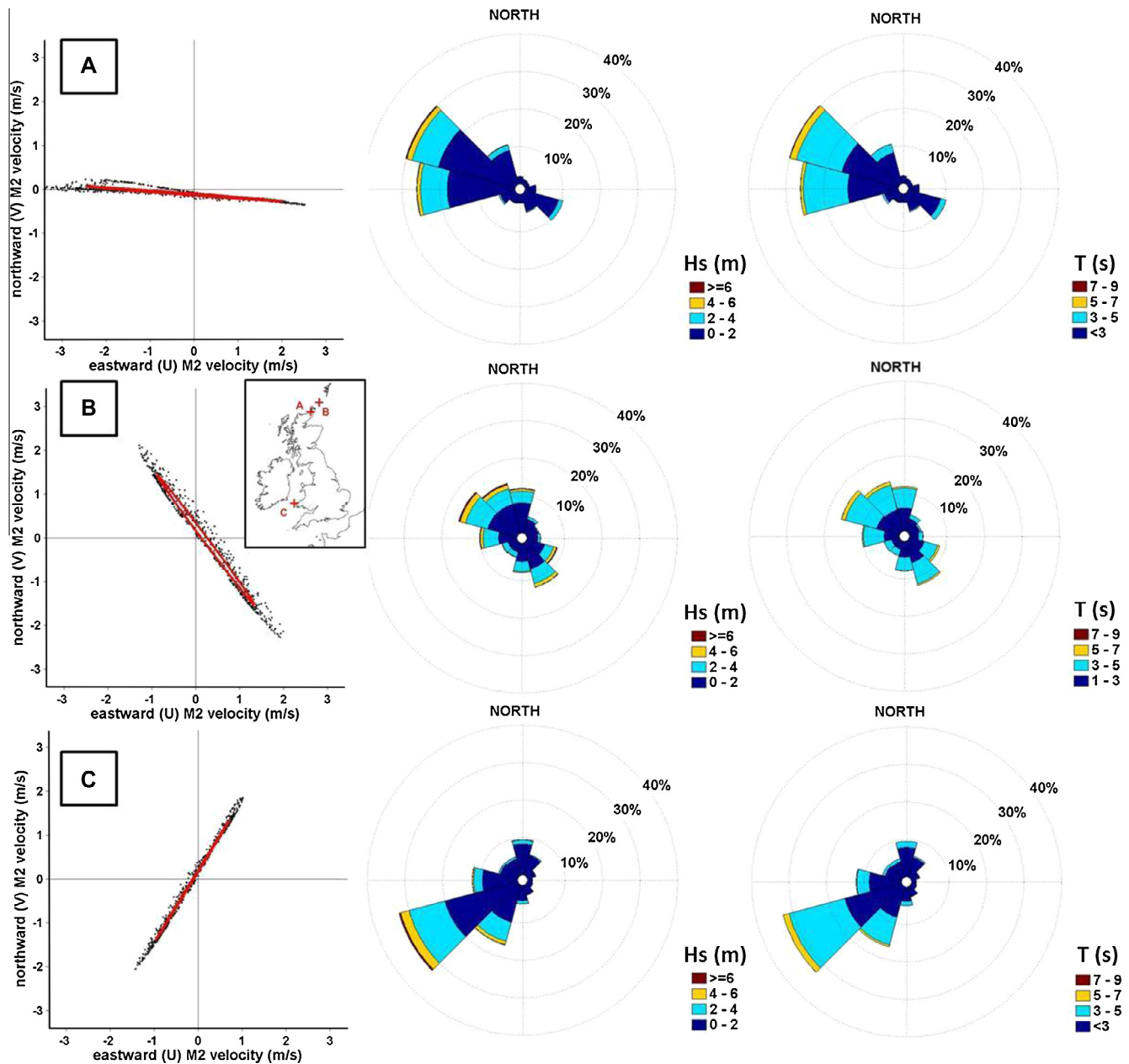
Fig. 3. Examples of the tide and wave climate at three potential tidal stream energy sites (A to C). Depth-averaged principal semi-diurnal lunar (M2) tidal velocity (black dots) simulated over 28 days, with the M2 tidal ellipse shown in red, and compared to the simulated 7 year (2005–2011) significant wave height (Hs), and SWAN wave model period output (T), averaged into $9 \times 40°$ bins at three potential tidal stream energy sites: (A) Pentland Firth west (site 1: 58.73°N & 3.34°W), (B) Orkney (site 6: 59.41°N & 2.24°W), and (C) Pembroke (site 10: 51.93°N & 5.45°W). (For interpretation of the references to colour in this figure legend, the reader is referred to the web version of this article.)

year wave climate, with maximum wave events typically being 2.25 m and 2 s greater in height and period (the average Hs being also 0.13 m higher). This examination of the wave and tidal conditions around the British Isles – a world leading marine energy resource – therefore brings into doubt the approach adopted by the majority of laboratory and CFD experiments, in which waves and tidal currents are assumed to be exclusively *inline* (waves following or opposing the flow).

2.5. Observations from the Pentland Firth

To further validate our simulations of the *oblique* wave-tidal current climate at tidal stream energy sites (Table 4), data from a Datawell Waverider buoy located in the Pentland Firth were analysed.

The Waverider buoy was deployed at 58.675°N and 3.279°W (located approximately between sites 1 and 2; see Fig. 1), between 16th January and 17th July 2012 (thus no complete autumn/winter observations were available) at ½ hourly intervals. The significant wave height (Hs), zero up-crossing wave period (Tz) and wave direction (°N) time-series of the Pentland Firth wave buoy is shown in Fig. 4. The M2 tidal ellipse was calculated at the corresponding location using our 3D ROMS UK tidal model. The angle of the M2 major current velocity axis was calculated to be 87° (relative to °N). As before (Section 2.4), the *inline* and *oblique* wave climate was calculated with a ±20° directional uncertainty tolerance, hence the *inline* and out-of-line wave climate (wave angle relative to tidal current flood-ebb axis >20°) was calculated and is presented in Table 5 and Fig. 4.

Table 3
The 7-year (2005 and 2011) *inline* wave climate to the major axis of the M2 tidal flow at 18 tidal stream energy sites (either waves following; INC ±20°, or waves opposing flow; inverse of INC ±20°). The occurrence of these *inline* wave events (%), the mean and standard deviation (s.d.) of height (*Hs*) and period (*T*), including the maximum *inline* wave event with the relative angle $\Delta\theta°$, as the smallest (irrespective of direction) angle between the axis of major tidal current and the wave direction.

Site	Occurrence (%)	Hs (m)		T (s)		Maximum event		$\Delta\theta°$
		Mean	s.d.	Mean	s.d.	Hs (m)	T (s)	
1	33	1.58	1.09	3.8	1.0	9.59	7.5	18
2	24	1.14	0.70	3.1	0.7	5.30	5.2	19
3	16	1.03	0.59	3.0	0.6	4.32	4.4	18
4	19	2.16	1.46	4.3	1.1	11.13	7.9	17
5	12	1.78	1.18	3.8	0.9	9.78	7.0	13
6	11	1.55	0.96	3.6	0.7	7.90	6.1	15
7	7	0.88	0.56	2.6	0.6	3.83	4.1	8
8	22	0.77	0.55	2.4	0.6	3.63	4.1	18
9	12	0.96	0.65	2.7	0.7	4.02	4.5	16
10	10	0.97	0.68	2.8	0.7	4.49	4.8	8
11	51	1.02	0.74	3.0	0.8	5.78	6.3	10
12	25	0.84	0.53	2.6	0.6	3.84	4.3	18
13	23	0.98	0.63	2.9	0.7	5.12	5.4	2
14	25	0.89	0.60	2.7	0.7	3.54	4.5	9
15	16	1.02	0.64	2.8	0.7	4.49	4.5	19
16	20	1.31	0.90	3.2	0.8	6.82	5.9	17
17	17	1.04	0.59	2.9	0.6	3.96	4.3	16
18	22	1.66	1.19	3.9	1.0	11.52	7.9	19

Table 4
The 7-year (2005 and 2011) *oblique* wave climate to the major axis of the M2 tidal flow at 18 tidal stream energy sites (i.e. not *inline* with the tidal flow ±20°). The occurrence of these *inline* wave events (%), the mean and standard deviation (s.d.) of height (*Hs*) and period (*T*), including the maximum *oblique* wave event with the relative angle $\Delta\theta°$, as the smallest (irrespective of direction) angle between the axis of major tidal current and the wave direction.

Site	Occurrence (%)	Hs (m)		T (s)		Maximum event		
		Mean	s.d.	Mean	s.d.	Hs (m)	T (s)	$\Delta\theta°$
1	67	1.29	1.00	3.3	1.0	9.48	7.4	28
2	76	1.13	0.80	3.0	0.8	7.08	6.1	26
3	84	1.17	0.78	3.3	0.8	6.53	6.3	68
4	81	2.03	1.39	4.1	1.0	11.91	8.1	24
5	88	2.09	1.44	4.1	1.0	11.70	8.0	61
6	89	2.02	1.32	4.1	1.0	9.79	7.5	44
7	93	1.23	0.89	3.1	0.8	7.34	6.1	77
8	78	0.96	0.71	2.7	0.7	4.89	4.9	59
9	88	1.26	0.99	3.1	0.9	7.66	6.2	86
10	90	1.56	1.20	3.5	1.0	10.40	7.5	81
11	49	0.59	0.46	2.2	0.6	3.26	4.3	20
12	75	1.27	1.03	3.1	1.0	9.15	7.2	42
13	77	0.98	0.64	2.8	0.7	4.63	5.2	27
14	75	0.81	0.56	2.6	0.6	4.35	4.5	59
15	84	1.11	0.81	2.9	0.8	8.02	6.6	57
16	80	1.33	1.04	3.3	0.9	11.09	7.9	42
17	83	1.29	0.92	3.3	0.9	9.70	7.5	56
18	78	1.76	1.30	3.8	1.1	12.49	8.4	26

Waves were observed to be at an angle (*oblique*) to the simulated tidal flow for the majority (90%) of the 6 month record; with a mean *oblique* significant wave height (*Hs*) of 1.11 m and zero up-crossing wave period (T_z) of 6s, compared to a mean *inline* *Hs* of 0.62 m and T_z of 5s. Further, the maximum oblique wave event (*Hs* = 5.45 m) was much greater than the *inline* counter part (*Hs* = 1.84 m); see Table 5. The 7-year modelled wave climate at Pentland Firth (i.e. between sites 1 and 3) cannot be directly compared to the 6 month observation period because of a difference in simulation dates and time-series length (i.e. modelled period between 2005 and 2011, whilst the observation period was between January 2012 and July 2012). However, as the wave model is already well validated [2,52], we can quantitatively compare observations to model results – as shown in the appendix. For

example, we estimate an 88% maintenance window based on the observed time-series (see Fig. 4) – which is very close to our maintenance window estimations for sites 1 to 3 in the Pentland Firth (79–88% – see Table 2). Moreover, the modelled and observed wave climates were similar; both in the frequency of *oblique* wave events (84% simulated at site 3 compared to 90% observed), and mean wave height (simulated *Hs* of 1.13 m to 1.29 m in the Pentland Firth compared to an observed mean *Hs* of 1.11 m); see Tables 3 and 5. Therefore, based on wave observations in the Pentland Firth (Fig. 4), and the simulated wave climate at 18 potential tidal stream energy sites around the British Isles (see Table 4 and Fig. 2), we conclude that a significant oblique wave climate can be present at tidal stream energy sites.

3. Effect of waves on tidal currents

The effect of waves upon the tidal velocity profile, and thus the tidal stream power available, was investigated for an idealized symmetrical headland, based on a modified classical headland test case [56]. A dynamically coupled tide-wave model was applied to this idealised headland domain, with characteristics similar to that of typical first generation tidal stream energy sites (in tidal velocities, wave climate, and water depths). A curvilinear grid (minimum grid size of 110 m by 92 m at the headland tip, maximum grid size of 1990 m by 1690 m offshore) was used to discretize a domain 50 km (east–west) by 25 km (north–south), with a parabolic headland running along the southern boundary, and depth increasing linearly from a minimum of 4 m (at the headland) to a constant depth of 40 m, 3 km offshore – see Fig. 5.

The direct effect on the tidal stream energy resource was calculated as a change in the net power available over a tidal cycle due to wave-induced modification of the tidal velocity. An M2 tidal flow (from 0.43 m/s to 0.5 m/s at the northern edge) and elevation (0.6–0.71 m), at the west and eastern boundary are imposed as a clamped free surface open radiation condition (see https://www.myroms.org/wiki/index.php/TEST_HEAD_CASE). The phase difference between the western and eastern boundary is such that the system acts like a standing wave (180° out-of-phase), with a node (almost zero free-surface amplitude) at the headland, where depth-averaged peak velocities of ∼2 m/s are generated.

The wave conditions applied as boundary conditions to the idealized headland domain of Fig. 5 were derived from the 7-year (2005–2011) SWAN northwest European shelf sea wave climate (see Fig. 6). We use the wave climate of site 1 (western Pentland Firth) as a typical tidal stream energy site because the mean wave height was close (0.06 m) to the average *Hs* of all sites (see Table 2). Therefore, based on the relationship between simulated wave height (*Hs*) and period (*T*) at site 1, the upper limit of swell waves (longer period) and storm wave events (shorter period) were derived (as shown in Fig. 6 and Table 6), and used to force the dynamically coupled wave-tide idealized headland model (see Fig. 6 and Section 3.1). Two boundary wave direction scenarios were imposed to account for wave direction: "north" (open northern boundary, waves propagating south) to simulate an *oblique* wave event, and "east" (open eastern boundary, waves propagating west) to simulate an *inline* wave event.

3.1. The dynamically coupled wave-tide modelling system

Dynamically coupled wave-tide models simulate the additional conservative and non-conservative forces; for example momentum and mass fluxes induced by waves (through stokes drift, radiation stress and wave roller terms in addition to the tidal flow), as well as the current induced Doppler shift in frequency and phase speed of the surface waves (e.g., [27,47]). Therefore, a dynamically cou-
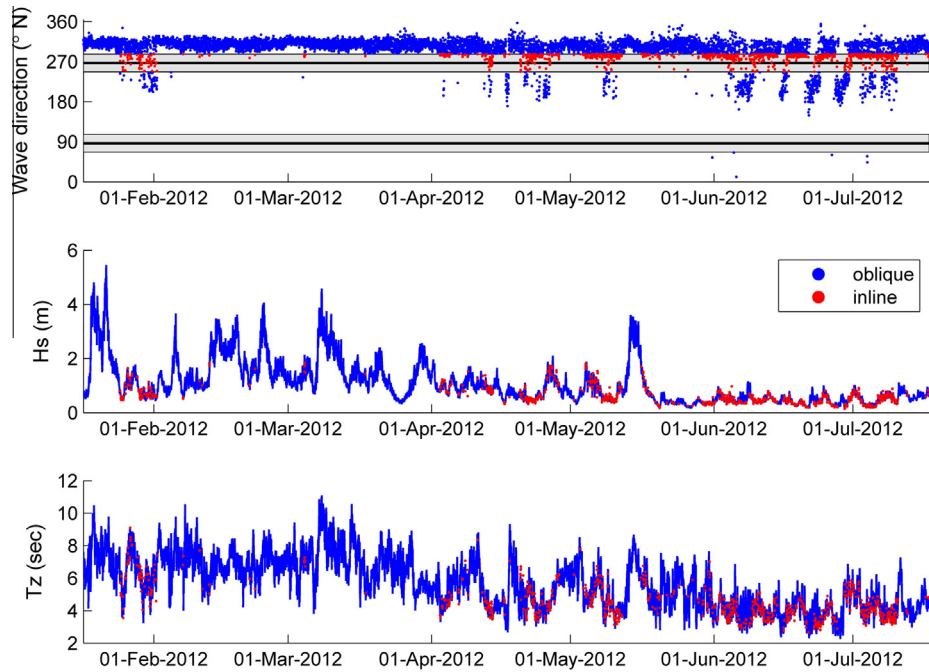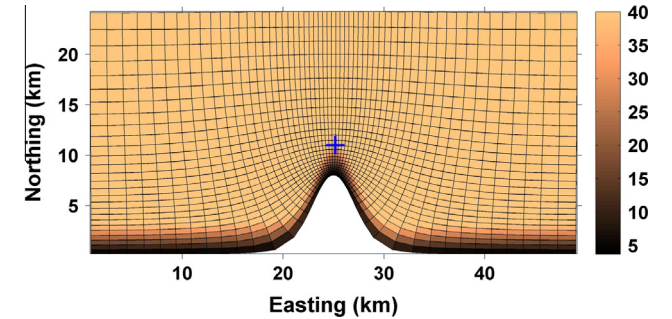
Fig. 4. The Waverider buoy observed Pentland Firth (3.279°W, 58.675°N) significant wave height (*Hs*), zero-upcrossing wave period (*Tz*) and peak wave direction (from °N) between 13th January 2012 and 18th July 2012. The wave climate has been split into wave events propagating *inline*, shown in red (either propagating <20° with or against the direction of the major axis of the M2 tidal flow), and oblique, shown in blue (propagating at an angle of >20° from the direction of M2 tidal flow), wave events. The inclination ±20° of the simulated M2 tidal ellipse (and its inverse angle) is shown as the grey shaded area in the top panel. (For interpretation of the references to colour in this figure legend, the reader is referred to the web version of this article.)
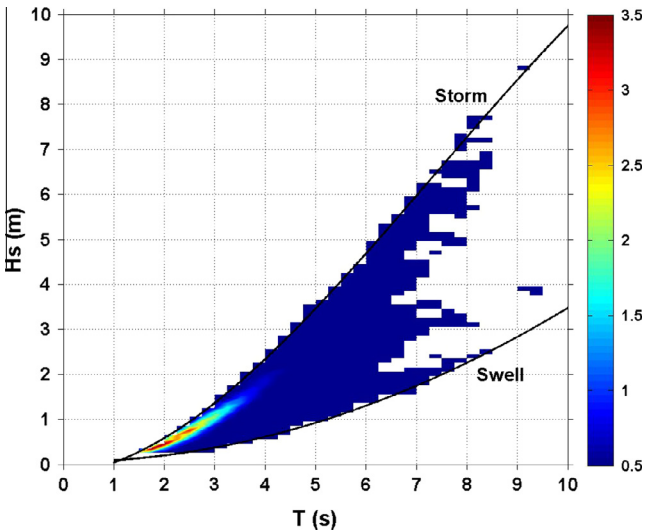
Table 5
The significant wave height (*Hs*) and zero-upcrossing wave period (*Tz* to the nearest integer) wave climate (including standard deviation; s.d) observed in the Pentland Firth (3.2792°W, 58.675°N) between 13th January 2012 and 18th July 2012. The wave climate has been split into wave events propagating *in-line* (either propagating with or against the tidal flow) and *oblique* (traveling at an angle of >20° or more from the direction of tidal flow).

	Oblique	*Inline* (±20°)
Occurrence	90%	10%
Mean (*Hs*)	1.11 m	0.62 m
s.d. (*Hs*)	0.80 m	0.33 m
Mean (*Tz*)	6 s	5 s
s.d. (*Tz*)	2 s	1 s
max (*Hs*)	5.45 m	1.84 m
Corresponding *Tz* of max	9 s	7 s

Fig. 6. The frequency (%) of wave conditions simulated over a 7 year period (2005–2011) at the Pentland Firth west site (58.73°N & 3.34°W). Wave conditions were averaged into 0.1 m significant wave height (*Hs*) and 0.25 s wave period (*T*) bins to calculate the frequency. Upper limit of the observed "swell" (longer period) and "storm" (shorter period) wave events is indicated with black lines.

Fig. 5. Idealized tidal stream energy headland model domain and bathymetry (*m*) used in the 3D dynamically coupled COAWST model. The position of the offshore point where tidal velocity profiles were analysed is shown as a blue cross.

pled model approach allows the simulation of non-linear interactions between the effect of tide on waves (e.g., [3,7]), and the effect of waves on currents [57].

One successful example of a dynamically coupled model is the Coupled Ocean Atmosphere Wave Sediment Transport (COAWST) model. The COAWST modelling system dynamically couples ROMS (tide), WRF (Weather Research and Forecasting atmospheric model), and SWAN (waves) models together using the Model Coupling Toolkit [57,58]. A number of dynamically coupled models have been developed that can simulate the interaction between waves and tides (e.g., [59]). We chose COAWST because it is highly flexible with many dynamical parameterization options (*cpp*

Table 6
Wave scenarios propagated into the dynamically coupled (wave-tide) COAWST model (at north and east boundaries), used to simulate the effect of waves upon the tidal velocity profile at an idealised headland tidal stream energy site for a "swell" or "storm" wave cases.

Wave height (m)	Storm wave period (s)	Swell wave period (s)
0.0	0.0	0.0
0.3	1.1	2.1
0.5	1.9	3.6
1.0	2.6	5.2
2.0	3.7	7.5
3.0	4.6	9.3
4.0	5.5	10.8

options), has an active user community, and has been successfully applied to study wave energy resource in European waters (e.g., [6]).

The interaction between velocity, turbulence, and the bottom boundary layer is parameterised in COAWST through bed shear stress calculations [47,58]. The GLS turbulence model used by COAWST includes wave breaking and wave effects on current (WEC) vortex-force parameterisation [18]. We use the WEC_MELLOR [60] parameterisation of radiation stress terms for waves on currents. The interaction between waves and bed shear stress is parameterised by a number of "BBL" (Bottom Boundary Layer) options [27]. The most recent BBL option, SSW_BBL [47], calculates the artificial bed roughness (Z_0) from wave-current interaction based on median sediment grain size (D_{50}). Coarse sand with a D_{50} of $\sim$3 mm or more has been observed in high flow regions typical of tidal stream energy sites (e.g., [61,62]) and is consistent with that predicted based on the threshold of motion; therefore, we use the SSW_BBL option assuming a grain size of 3 mm in our COAWST simulations.

The idealised headland test case was simulated with the COAWST using 2.9 GHz processors in the HPC Wales Sandy Bridge system (www.hpcwales.co.uk). Velocities and wave climate information was extracted at 15 min intervals, for one complete tidal cycle after a 36 h model spin up. Therefore, the potential effect of waves on tidal velocities was simulated for a realistic tidal stream energy site for a number of wave scenarios (Table 6) and directions. Net tidal stream power density available over a tidal cycle was calculated by integrating the power density (P_t) time-series calculated from the COAWST simulated depth averaged velocity ($\bar{u}_t$) multiplied by density (ρ, we assume 1025 kg/m^3): $\int_0^{12.42h} P_t = \frac{1}{2} (\bar{u}_t)^3 dt$; hence, the theoretical effect of waves upon the tidal resource could be calculated without assuming a turbine area (i.e. kW/m^2).

3.2. Wave-tide coupled model results

The time-evolution of the surface elevation and depth averaged tidal velocity field simulated with COAWST (no waves) is shown in Fig. 7 for one complete tidal cycle. The simulated tidal conditions resulted in a standing wave with a node offshore of the headland; where changes in surface elevation are small, but the horizontal tidal velocities are large and increased further as the flow accelerates past the headland constriction (see Fig. 7). The deceleration of the tidal flow past the headland results in an eddy forming in the lee of the headland, which is advected past the headland and dissipates as the tidal flow reverses and accelerates; see Fig. 7.

Velocity profiles were extracted at a point offshore of the headland (25.16 km Easting and 11 km Northing), which we assume to be suitable for a tidal energy array; where the depth averaged tidal velocity was close to 2 m/s in 40 m water depth, and in close enough proximity to shore for feasible grid connection. The COAWST simulated difference in tidal velocity profiles when an "east"

(i.e. westward propagating) swell wave case of 4 m wave height (Hs) and 11 s wave period (T), were forced at the eastern boundary is shown in Fig. 8. An average wave height of 3.79 m (Hs) and period (T) of 9s was recorded at the headland tidal energy site, because of COAWST simulated wave attenuation. Wave direction at the analysis site (see Fig. 7) varied between 78°N and 92°N (mean direction of 83°N) due to wave-tide interaction and bathymetry refraction (e.g. [7]). Therefore, we assume "east" wave conditions to be *inline* to the tidal flow.

The presence of $\sim$4 m swell waves modified the wave-averaged tidal velocity at an idealized tidal stream energy site in both the U (eastwards) and V (northwards) components; see Fig. 8. Waves were forced from the eastern boundary, propagating westwards; hence we assume "wave opposing flow conditions" when the U component of tidal velocity is positive and call this wave direction scenario "east". The depth-averaged peak flood tide velocity at the headland (4–6 h of Fig. 8) was reduced in the presence of waves, and the phase of the depth-averaged ebb tide velocity (8–12 h) was also shifted; see Fig. 8. In accelerating tidal flows (either waves opposing or waves following current), we found the presence of large swell waves modified the tidal velocity profile, with the biggest increase in the upper water-column. In both the peak-velocity stage of the flood and ebb tidal cycle (profiles 2 and 5 of Fig. 8 respectively), the presence of swell waves decreased tidal velocities throughout the water-column.

If we assume the magnitude of tidal velocity is most important for characterizing the tidal stream energy resource (as designs will allow tidal turbines to face the direction of flow), we can investigate the simulated change to the wave averaged tidal velocity profile under the effect of various wave scenarios and directions. The wave conditions of Table 6 (forced at the eastern and northern boundaries) indicated a phase shift in the ebb tidal current, and a decrease in peak flood tide velocity; with larger wave heights (Hs) increasing (1) the ebb tidal current phase lag, and (2) the suppression of peak flood tide velocities at the analysis site (25.16 km Easting and 11 km Northing; see Fig. 5).

The tidal stream power density (P) available at height z in the water column was calculated using the equation $P_{(z)} = \frac{1}{2} \rho_z^3$ for each COAWST simulated tidal current speed profile (u_z) output time step (every 15 min): note, the square of the tidal current speed at depth z (u_z) is calculated as the sum of the square of the tidal current components (northwards and eastwards). The vertical tidal stream power density over a tidal cycle is shown in Fig. 9, alongside the depth averaged tidal velocity, which demonstrates that a small change in tidal velocity results in a large change in the available power, since tidal stream power is a function of the velocity cubed. Therefore, although 4 m *inline* swell waves reduced the depth-averaged tidal velocity by approximately 0.2 m/s during the peak flood tide, the power available near the surface at the same time was reduced by up to 59% (at 5 h in Fig. 9). The simulated wave-induced phase shift of the ebb tide velocity (Fig. 9) resulted in a negligible change to the net tidal stream power available over the course of a tidal cycle – as the increase of power with waves under accelerating ebb tide flow effectively cancels out the simulated decrease of power with the presences of waves in the decelerating ebb tide flow. However, the simulated wave-induced reduction in peak flood tidal velocity dominates the change in the tidal stream power available over the course of a tidal cycle; see Fig. 9(a).

The simulated wave induced differences of tidal velocity and power shown in Figs. 8 and 9 are for one location (25.16 km Easting and 11 km Northing); therefore, we investigated the change to the tidal stream energy resource throughout the domain. The net power density (kW/m^2 available over a tidal cycle) without waves, and with the *inline* 4 m swell wave case, is shown in Fig. 10. The difference of net power available over a tidal cycle due to the pres-
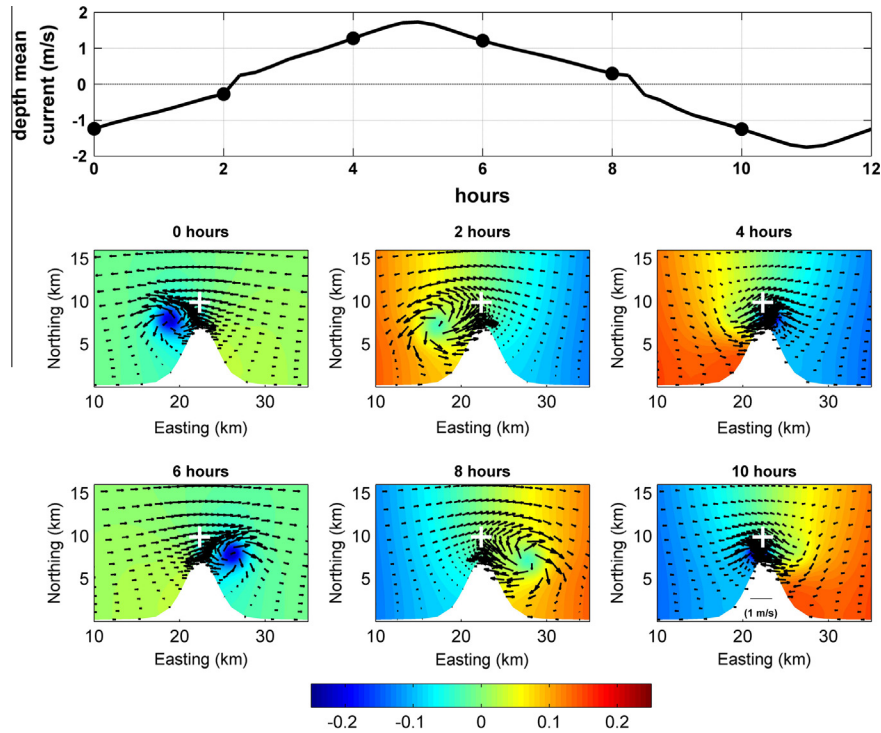
Fig. 7. The COAWST simulated depth averaged tidal current speed (flood is positive, ebb tide is negative) offshore of an idealised headland tidal stream energy site (position marked with a +) for one M2 tidal cycle and "no wave" condition. Horizontal tidal elevation (colour scale, in metres) and depth averaged-velocity current vector fields are shown in the bottom six panels at: 0, 2 4, 6, 8, and 10 h.
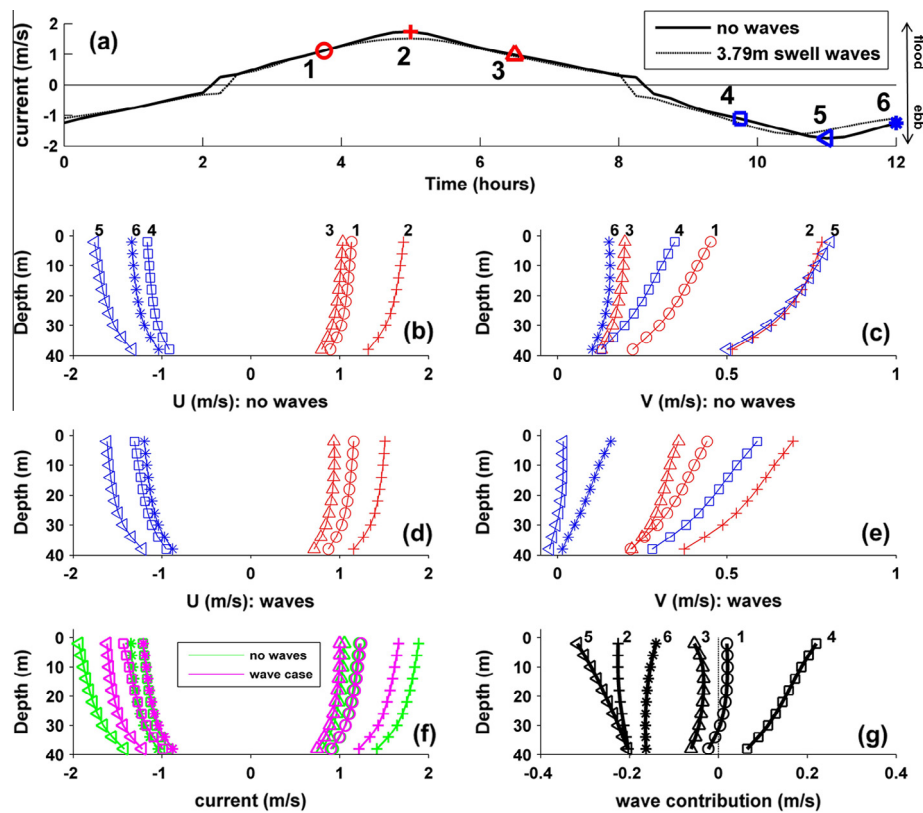
Fig. 8. The COAWST simulated tidal velocity difference (10 vertical layers) under the presence of 4 m "swell" (11 s in period) when waves propagate westwards in the model domain, which decrease to 3.79 m 9 s waves offshore of the idealised headland. The top panel (a) shows the depth-averaged tidal velocity with the negative sign denoting a westward flowing, ebb tide. The U (east–west) and V (north–south) components of the velocity profile are shown for six points over the tidal cycle in panels b and c, respectively. Further, the U (panel d), and V (panel e) components of the simulated velocity profile under the presence of westward propagating 3.79 m swell waves are shown, and the current (velocity profile irrespective of direction) is compared in panel f. The difference in tidal velocity compared to the "no waves" case (i.e. the contribution of waves to the tidal current) is shown in panel g.
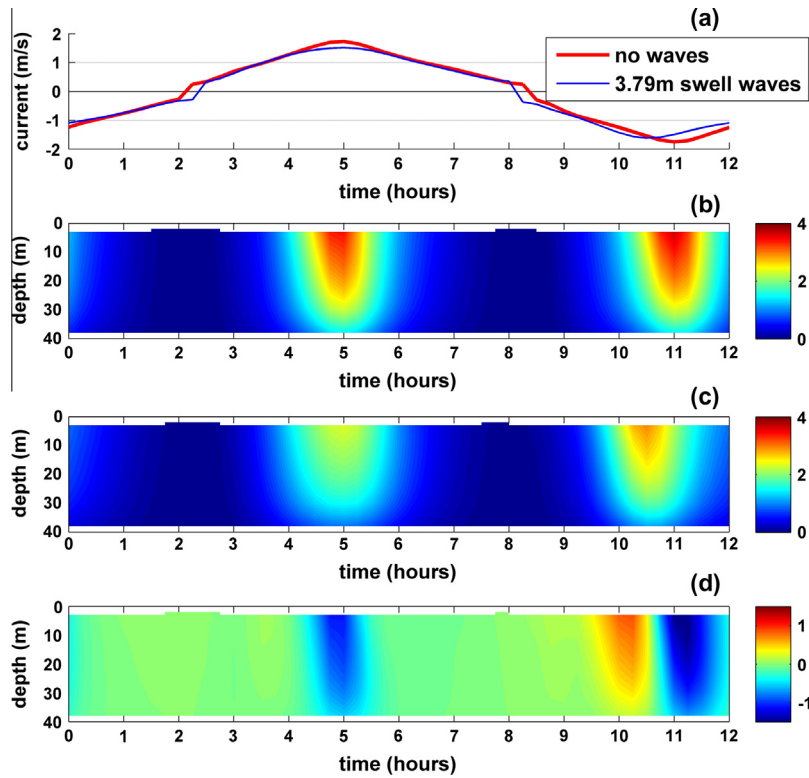
Fig. 9. The tidal stream power density (kW/m²) offshore of an idealised tidal stream energy headland (b), and under the presence of 3.79 m swell waves propagating westwards (4 m and 11 s at the east model boundary) over a tidal cycle (c). The difference in the power available due to waves is shown in panel d. The depth averaged tidal velocity (negative sign denotes a westward tidal flow) is shown in the top panel.

ence of such waves (Hs = 4 m Ts = 11 s) was calculated as a percentage (negative values denote waves reduce the tidal stream resource), and is also shown in Fig. 10.

Spatial variability to the influence of waves on the tidal stream energy resource was found (Fig. 10c). It appears that waves alter the strength and position of the headland eddy systems; most likely because SWAN simulated waves changed the parameterised COAWST turbulence scheme. The presence of waves also increased the net tidal stream power on the eastern headland shore (Fig. 10c) due to near-shore processes, which is of little consequence to the tidal stream energy resource region (i.e. the red area of Fig. 10a). Of more interest to the tidal stream energy industry is the reduction in the area and magnitude of the tidal energy resource in our COAWST simulation; see Fig. 10.

If we assume that tidal stream energy developers are primarily interested in regions where peak depth-averaged tidal velocities exceed 1.5 m/s, the percentage difference in the net power available over a tidal cycle can be calculated for this region of interest (ROI). The wave scenarios of Table 6 were forced at the eastern (propagating westward scenarios) and northern (propagating southward scenarios) COAWST boundaries. The impact of waves on the theoretical tidal stream resource is shown in Fig. 11 for both *inline* (east) and *oblique* (north) wave direction scenarios. Wave-tide interaction altered the wave direction and size in our COAWST simulations – therefore, the modal average wave height for the ROI and averaged over a tidal cycle was used in Fig. 11, and subsequent analysis.

Considering the 7-year average wave height (H) simulated at the 18 selected sites (see grey shaded area of Fig. 11), all wave direction and period scenarios resulted in a decrease of the tidal resource (approximately between −1% and −21%). Wave conditions that were propagating *inline* to the tidal flow ("east" waves) were found to increase the net power available for small (<0.6 m)

wave conditions (both swell and storm). North wave events reduced the net power available compared to the *inline* ("east") scenarios; however simulated wave heights (H) were not as attenuated as east scenarios (due to domain dimensions and wave-tide interaction), which would have effected the magnitude of tidal current modification. Linear regression of the percentage change to the theoretical net tidal stream power available over a tidal cycle (ΔP) for each of the wave scenarios showed a strong correlation;

$\Delta P = -7.5H + 2.4$ (for "east" swell waves) R^2 of 96%

$\Delta P = -10.0H + 1.9$ (for "east" storm waves) R^2 of 99%

$\Delta P = -3.0H + 1.4$ (for "east" storm waves) R^2 of 84%

$\Delta P = -9.4H + 2.3$ (for "north" storm waves) R^2 of 98%

The spread of COAWST results in Fig. 11 highlights the complex non-linear and two-way interaction between tidal currents, wave height, wave period, and direction. However, if we group all wave scenarios together (increasing the degrees of freedom to 22), we still obtain a strong linear relationship: $\Delta P = -10.0H + 3.8$ (R^2 of 94%). Further, if we assume electricity can only be produced when tidal velocities exceed a typical cut-in speed of 1.0 m/s (i.e. only sum the net power if the velocity exceeds 1.0 m/s), we find the *practical* resource is also reduced (and reduced to a greater extent than the theoretical resource) by the presence of waves: $\Delta P_{practical} = -10.8H + 4.3$ (R^2 of 94%).

The Prandle and Wolf [39] tidal current – wave height relationship was applied to the COAWST simulated no wave condition, assuming a uniform spatial change to tidal velocity. We find this Prandle and Wolf relationship is broadly consistent with our simulated results (see dotted line on Fig. 11). Although wave direction does influence the tidal stream resource, we find the presence of waves reduces both the theoretical and practical tidal stream
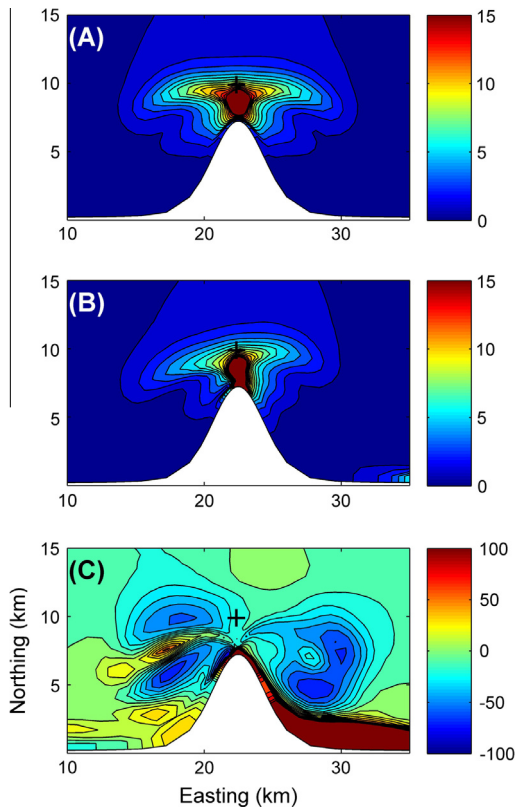
Fig. 10. The net power density available over a tidal cycle (kW/m^2) calculated using the COAWST simulated depth averaged velocity time-series without waves (A) and under the presence of westerly propagating 4 m "swell" waves (B). The difference (%) in the net power available over a tidal cycle due to waves is also shown (C). The location of the velocity profile analysis (Fig. 7) and the power density time-series (Fig. 8) is shown as a cross (+).
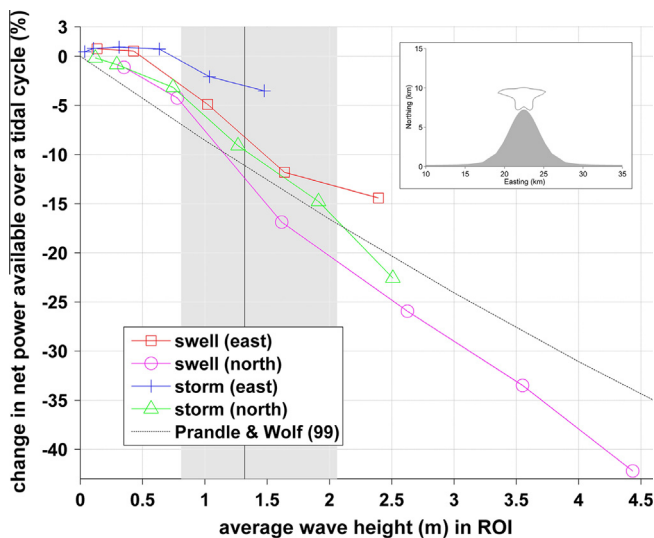
Fig. 11. The difference in the net power available over a tidal cycle in the region of interest (ROI) of the COAWST domain (where peak velocities exceed 1.5 m/s, shown as a black line in the box) – when the simulated of tidal velocities are modified by waves. The theoretical change to tidal stream power available due to wave-induced reduction in M2 tidal velocity observed by Prandle and Wolf (1999) is also provided for comparison.

resource in proportion to wave height. Therefore, computationally expensive dynamically coupled wave-tide models may not be required to determine site specific resource estimates if the wave

climate is known – however much more research is required to confirm this conclusion.

4. Discussion

Spatial variability within the wave climate was found between our selected tidal stream energy sites using a 7-year (2005–2011) SWAN simulation. The number of hours when we assume maintenance of tidal energy arrays could take place was calculated (duration when $Hs < 2$ m), based on current offshore wind farm guidelines for maintenance boat access [55]. We found the amount of time when maintenance could occur varied between 60% and 90% of the 7-year simulation across the 18 selected sites (see Table 2 and Fig. 2 for exceedance plot of wave height for a number of potential sites). Moreover, large wave events above 10 m and 10s were found to occur at many sites, which will require tidal turbines to enter a "survival mode" and cease electricity production; thus potentially effecting operability and reliability of tidal turbines. Therefore, correctly selecting the location of a tidal stream energy site, with a consideration of the wave climate, could be important for successful array deployment.

Studies of turbine wake effects, as well as fatigue and extreme loading to the tidal turbine, assume that waves propagate *inline* to the tidal flow (e.g., [15,16,18]). Significant wave events propagating at an angle oblique to the tidal flow (waves not travelling with or against the tidal current) were found at all of our 18 selected sites. For example, the 7-year simulated maximum wave height was not *inline* for the majority of sites (see Tables 3 and 4). Wave orthogonals tend to propagate normal to the coastline, whereas tidal currents tend to be aligned parallel to the coastline. Furthermore, shorter period waves are mainly affected by current refraction, whilst longer period waves are more affected by bathymetric refraction [7,63]. Indeed, only site 11 ("Bristol Channel") had an *inline* wave climate that was greater than the *oblique* wave climate. Therefore, any future studies of the interaction between a tidal turbine and realistic oceanographic conditions, or investigations into the performance of some offshore wave energy convertor types (see [64]), should consider for wave-tidal current misalignment. Moreover, future work should investigate the spatial dependence of relative wave angle around all tidal stream energy sites, including the relationship between relative wave angle and tidal current speed as well as relative wave angle and water depth.

A tolerance of ±20° in our *inline* wave climate estimation was used to account for sub-grid scale wave refraction, which, it appears from sensitivity test with our dynamically coupled wave-tide model, is an acceptable level of tolerance. Indeed, observations from the Pentland Firth (Fig. 4) confirms our hypothesis that waves often propagate at an angle oblique to the rectilinear tidal flow, and that extreme wave events are more likely to propagate at an angle *oblique* to the tidal flow. However, we believe that direct observations of both wave and current angles at tidal stream energy sites is obvious scope for future work to fully test this hypothesis, especially as we assume the ebb and flood tidal current to be 180° to each other, which may not be the case in regions of complex bathymetry.

Our dynamically coupled wave-tide simulation of an idealized headland tidal stream energy site demonstrates that waves reduce tidal velocities by a small amount in 40 m water depth, confirming previous observations [40], which is mainly attributed to waves increasing the apparent bed roughness (e.g., [28–31,40]). However, since tidal stream power is a function of velocity cubed, a small change in the tidal velocity resulted in a significant effect (i.e. above a 10% change) to the tidal stream power available over a tidal cycle, even for 1–2 m waves (the mean wave height over the 18 sites; see Tables 2 and 3); see Fig. 11. A strong linear rela-

tionship was found (R^2 94%) between the wave height and the net power available over a tidal cycle (both theoretical and practical tidal stream energy resource). Therefore, the wave climate, including wave direction (relative to the current), should be considered when selecting sites suitable for tidal stream energy arrays.

The relationship between waves and their effect on the tidal stream energy resource is complex, due to accelerating tidal flows and the interaction between tides and waves [3,34–40,63]. Therefore, a dynamically coupled modelling approach may be required – as suggested by Barbariol et al. for the wave energy resource [7]. However, a strong linear relationship between the simulated tidal resource and wave height was found in our study, which suggests a simpler approach could be sufficient if the wave climate is known – although further work is required to validate the simulated effect presented in this paper. Further, it should be noted that COAWST simulated velocity profiles are sensitive to bottom roughness parameterisation (e.g. choice of bottom drag formulation – see Warner et al., [47]), although sensitivity tests (not shown here) revealed the relationship between the tidal current profile modification due to bottom roughness (parameterised as a drag coefficient) and sediment type (parameterised as sediment grain size) was similar when including wave effects (i.e. the presence of waves decreased the velocities at all depths, but most noticeably near the surface – and this relationship increased with increasing bottom roughness). Hence, more research is required in the field of waves influencing the tidal stream power resource, including the stochastic nature of wave events to determine the likely annual impact to the resource (e.g. [6]), and the impact of tidal stream energy to the environment when including the wave climate (e.g. [52,65]). Moreover, observations at tidal stream energy sites of wave-tide conditions, including modification of tidal velocities, should be a priority for tidal stream energy research.

5. Conclusions

Previous research concludes waves indirectly affect the tidal stream energy resource, through the impact of storm waves affecting stresses on the turbine blades, support structure, and array configuration. Wave events that propagate at an angle oblique to the tidal flow were found at 18 tidal energy sites distributed across the British Isles (approximately 80% of the time), and the 7-year maximum wave event was found to be an *oblique* wave event at almost all of our selected sites. Therefore, wave angle should be considered in future studies which examine the interaction between tidal turbines and their environment. Furthermore, our results demonstrate that surface waves will have a significant impact upon the power available for tidal stream energy production, through altering tidal velocities (thus directly affecting the available resource), affecting maintenance schedules, and the number of days when electricity production cannot occur due to storms. Hence, a dynamically coupled wave-tide hydrodynamic model may be useful for accurate tidal stream resource assessment, although the simple linear method we present here may provide a good first order approximation. Finally, to develop the tidal stream energy industry further, we find that much research is needed to understand realistic oceanographic conditions at marine renewable energy sites, including publicly available current profile observations.

Acknowledgements

References

[1] Burrows R, Walkington IA, Yates NC, Hedges TS, Li M, Zhou JG, et al. Tidal energy potential in UK waters. Proc ICE-Maritime Eng 2009;162(4):155–64.

[2] Neill SP, Hashemi MR. Wave power variability over the northwest European shelf seas. Appl Energy 2013;106:31–46.

[3] Saruwatari A, Ingram DM, Cradden L. Wave-current interaction effects on marine energy converters. Ocean Eng 2013;73:106–18.

[4] Gant S, Stallard T. Modelling a Tidal Turbine in Unsteady Flow. in: Proceedings of the Eighteenth (2008) International Offshore and Polar Engineering Conference Vancouver, BC, Canada, July 6–11, 2008.

[5] Harrison GP, Wallace AR. Climate sensitivity of marine energy. Renewable Energy 2005;30(12):1801–17.

[6] Hashemi MR, Neill SP, Davies AG. A coupled tide-wave model for the NW European shelf seas, Geophysical and Astrophysical Fluid Dynamics, 2014, in press. http://dx.doi.org/10.1080/03091929.2014.944909

[7] Barbariol F, Benetazzo A, Carniel S, Sclavo M. Improving the assessment of wave energy resources by means of coupled wave-ocean numerical modelling. Renewable Energy 2013;60:462–71.

[8] Afgan I, McNaughton J, Rolfo S, Apsley D, Stallard T, Stansby P. Turbulent flow and loading on a tidal stream turbine by LES and RANS. Int J Heat Fluid Flow 2013;43:96–108.

[9] Mason-Jones A, O'Doherty DM, Morris CE, O'Doherty T. Influence of a velocity profile & support structure on tidal stream turbine performance. Renewable Energy 2013;52:23–30.

[10] Work PA, Haas KA, Defne Z, Gay T. Tidal stream energy site assessment via three-dimensional model and measurements. Appl Energy 2013;102:510–9.

[11] Nicholls-Lee RF, Turnock SR, Boyd SW. Application of bend-twist coupled blades for horizontal axis tidal turbines. Renewable Energy 2013;50:541–50.

[12] Davies P, Germain G, Gaurier B, Boisseau A, Perreux D. Evaluation of the durability of composite tidal turbine blades. Philos Trans Royal Soc A: Math, Phys Eng Sci 2013;371:20120187.

[13] Rourke O, Boyle F, Reynolds A. Tidal energy update 2009. Appl Energy 2010;87(2):398–409.

[14] Val DV, Chernin L, Yurchenko DV. Reliability analysis of rotor blades of tidal stream turbines. Rel Eng Syst Saf 2014;121:26–33.

[15] McCann G, Thomson M, Hitchcock S. Implication of site-specific conditions on the prediction of loading and power performance of a tidal stream device. In: 2nd International Conference on Ocean Energy (ICOE 2008), 15th – 17th October 2008, Brest France.

[16] Milne IA, Day AH, Sharma RN, Flay RGJ. Blade loads on tidal turbines in planar oscillatory flow. Ocean Eng 2013;60:163–74.

[17] Barltrop N, Varyani KS, Grant A, Clelland D, Pham XP. Investigation into wave-current interactions in marine current turbines. Proc Institut Mech Eng, Part A: J Power Energy 2007;221(2):233–42.

[18] Luznik L, Flack KA, Lust EE, Taylor K. The effect of surface waves on the performance characteristics of a model tidal turbine. Renewable Energy 2013;58:108–14.

[19] Dean RG, Dalrymple RA. Coastal processes with engineering applications. Cambridge University Press; 2002. p. 475.

[20] Holliday NP, Yelland MJ, Pascal R, Swail VR, Taylor PK, Griffiths CR, et al. Were extreme waves in the Rockall Trough the largest ever recorded? Geophys Res Lett 2006;33(5):L05613.

[21] Adcock TAA, Taylor PH, Yan S, Ma QW, Janssen PAEM. Did the Draupner wave occur in a crossing sea? Proc R Soc A 2011;467(2134):3004–21. http://dx.doi.org/10.1098/rspa.2011.0049.

[22] Galloway PW, Myers LE, Bahaj AS. Quantifying wave and yaw effects on a scale tidal stream turbine. Renewable Energy 2014;63:297–307.

[23] Batten WMJ, Bahaj AS, Molland AF, Chaplin JR. The prediction of the hydrodynamic performance of marine current turbines. Renewable Energy 2008;33(5):1085–96.

[24] Smith J. On surface gravity waves crossing weak current jets. J Fluid Mech 1983;134:277–99.

[25] Kenyon KE. Wave refraction in ocean currents. Deep Sea Res Oceanogr Abstr 1971;18(10):1023–34.

[26] McCann GN. Tidal current turbine fatigue loading sensitivity to waves and turbulence – a parametric study. In: Proc. 7th European Wave and Tidal Energy Conference, Porto, Portugal, 2007.

[27] Kumar N, Voulgaris G, Warner JC, Olabarrieta M. Implementation of the vortex force formalisation in the coupled ocean-atmosphere-wave-sediment transport (COAWST) modeling system for inner shelf and surf zone applications. Ocean Model 2012;47:65–95.

[28] Grant WD, Madsen OS. Combined wave and current interaction with a rough bottom. J Geophys Res 1979;84(C4):1797–807.

[29] Teles MJ, Pires-Silva AA, Benoit M. Numerical modelling of wave current interactions at a local scale. Ocean Model 2013;68:72–87.

[30] Yang S, Tan SK, Lim SY, Zhang SF. Velocity distribution in combined wave-current flows. Adv Water Resources 2006;29:1196–208.

[31] Groeneweg J, Klopman G. Changes of the mean velocity profiles in the combined wave-current motion described in a GLM formulation. J Fluid Mech 1998;370:271–96.

[32] Draper S, Borthwick AGL, Houlsby GT. Energy Potential of a tidal fence deployed near a coastal headland. Philos Trans Royal Society 2013;371:20120176 [Part A].

[33] Bryden IG, Couch SJ. ME1—marine energy extraction: tidal resource analysis. Renewable Energy 2006;31:133–9.

[34] Kemp PH, Simons RR. The interaction between waves and a turbulent current: waves propagating with the current. J Fluid Mech 1982;116:227–50.

[35] Kemp PH, Simons RR. The interaction between waves and a turbulent current: waves propagating against the current. J Fluid Mech 1983;130:73–89.

[36] Musumeci RE, Cavallo L, Foti E, Scandura P. Waves plus currents crossing at a right angle: experimental investigation. J Geophys Res 2006; Oceans (1978–2012), 111(C7).

[37] Olabarrieta M, Medina R, Castanedo S. Effects of wave-current interaction on the current profile. Coast Eng 2010;57:643–55.

[38] Davies AG, Soulsby RL, King HL. A numerical model of the combined wave and current bottom boundary layer. J Geophys Res 1988;93:491–508.

[39] Prandle D, Wolf J. Some observations of wave-current interaction. Coast Eng 1999;37:471–85.

[40] Prandle D. The influence of bed friction and vertical eddy viscosity on tidal propagation. Cont Shelf Res 1977;17(11):1367–74.

[41] Couch SJ, Bryden I. Tidal current energy extraction: hydrodynamic resource characteristics. Proc IMechE Part M: Eng Maritime Environ 2006;220:185–94.

[42] Sánchez M, Carballo R, Ramos V, Iglesias G. Tidal stream energy impact on the transient and residual flow in an estuary: A 3D analysis. Appl Energy 2014;72:167–77.

[43] Shchepetkin AF, McWilliams JC. A method for computing horizontal pressure-gradient force in an oceanic model with a nonaligned vertical coordinate. J Geophys Res 2003;108(c3):3090. http://dx.doi.org/10.1029/2001JC001047.

[44] Shchepetkin AF, McWilliams JC. Regional Ocean Model System: a split-explicit ocean model with a free-surface and topography-following vertical coordinate. Ocean Model 2005;9:347–404.

[45] Haidvogel DB, Arango H, Budgell WP, Cornuelle BD, Curchitser E, Di Lorenzo E, et al. Ocean forecasting in terrain-following coordinates: Formulation and skill assessment of the Regional Ocean Modeling System. J Comput Phys 2008;227(7):3595–624.

[46] Neill SP, Hashemi MR, Lewis MJ. The role of tidal asymmetry in characterizing the tidal energy resource of Orkney. Renewable Energy 2014;68:337–50.

[47] Warner JC, Sherwood CR, Signell RP, Harris CK, Arango HG. Development of a three-dimensional, regional, coupled wave, current, and sediment-transport model. Comput Geosci 2008;34:1284–306.

[48] Warner JC, Sherwood CR, Arango HG, Signell RP. Performance of four turbulence closure methods implemented using a generic length scale method. Ocean Model 2005;8:81–113.

[49] Lyard F, Lefevre F, Letellier T, Francis O. Modelling the global ocean tides: modern insights from FES2004. Ocean Dyn 2006;56(5–6):394–415.

[50] Carrère L, Lyard F, Cancet M, Guillot A, Roblou L. FES2012: A new global tidal model taking advantage of nearly 20 years of altimetry. Proceedings of meeting "20 Years of Altimetry", Venice 2012.

[51] Booij N, Ris RC, Holthuijsen LH. A third-generation wave model for coastal regions – 1. Model description and validation. J Geophys Res 1999;104:7649–66.

[52] Robins PE, Lewis MJ, Neill SP. Impact of tidal-stream arrays in relation to the natural variability of sedimentary processes. Renewable Energy 2014;72:311–21.

[53] Pawlowicz R, Beardsley B, Lentz S. Classical tidal harmonic analysis including error estimates in MATLAB using T_TIDE. Comput Geosci 2002;28:929–37.

[54] Akpinar A, Vledder GP, Komurcu MI, Ozger M. Evaluation of the numerical wave model (SWAN) for wave simulation in the Black Sea. Cont Shelf Res 2012;50–51:80–99.

[55] Dowell J, Zitrou A, Walls L, Bedford T, Infield D. Analysis of Wind and Wave Data to Assess Maintenance Access to Offshore Wind Farms. 2013. www.strath.ac.uk accessed 18/03/14.

[56] Signell RP, Geyer WR. Transient eddy formation around headlands. J Geophys Res 1991;96(C2):2561–75.

[57] Warner JC, Perlin N, Skyllingstad ED. Using the model coupling toolkit to couple earth system model. Environ Modell Software 2008;23:1240–9.

[58] Warner JC, Armstrong B, He R, Zambon JB. Development of a coupled ocean-atmosphere-wave-sediment transport (COAWST) modelling system. Ocean Model 2010;35:230–44.

[59] Brown JM, Souza AJ, Wolf J. An 11-year validation of wave-surge modelling in the Irish Sea using a nested POLCOMS-WAM modelling system. Ocean Model 2010;33:118–28.

[60] Malarkey J, Davies AG. A non-iterative procedure for the Wiberg and Harris (1994) oscillatory sand ripple predictor. J Coastal Res 2003;19:738–9.

[61] Easton MC, Harendza A, Woolf DK, Jackson AC. Modelling the hydrodynamic Characterisation of Tidal Flow in the Pentland Firth, European Wave and Tidal Energy Conference 2011 Southampton.

[62] Robins PE, Neill SP, Davies AG. The impact of tidal energy extraction on the morphodynamics of the Irish Sea. In: 4th International Conference on Ocean Energy, 17 October, Dublin 2012.

[63] Mason D. A case study of wave-current interaction in a strong tidal current. J Phys Oceanogr 1996;26:359–72.

[64] Keskin Citiroglu H, Okur A. An approach to wave energy converter applications in Eregli on the western Black Sea coast of Turkey, Applied Energy, Available online 12 June 2014, ISSN 0306–2619.

[65] Lewis M, Neill S, Elliott A. Inter-annual variability of two contrasting offshore sand banks in a region of extreme tidal range. J Coastal Res 2014, in press. http://dx.doi.org/10.2112/JCOASTRES-D-14-00010